Uncertainty Quantification of Resonant Ultrasound Spectroscopy for Material Property and Single Crystal Orientation Estimation on a Complex Part

John C. Aldrin[2, a)], Alexander Mayes[3, b)], Leanne Jauriqui[3, c)], Eric Biedermann[3, d)], Julieanne Heffernan[3, e)], Richard Livings[3, f)], Brent Goodlet[4, g)]
Siamack Mazdiyasni[1, h)]

[1]*Air Force Research Laboratory (AFRL/RXCA), Wright-Patterson AFB, OH 45433, USA*
[2]*Computational Tools, 4275 Chatham Avenue, Gurnee, IL 60031, USA*
[3]*Vibrant Corporation, Albuquerque, NM 87113, USA*
[4] *University of California, Santa Barbara, Santa Barbara, CA 93106, USA*

[a)] Corresponding author: aldrin@computationaltools.com

Abstract. A case study is presented evaluating uncertainty in Resonance Ultrasound Spectroscopy (RUS) inversion for a single crystal (SX) Ni-based superalloy Mar-M247 cylindrical dog-bone specimens. A number of surrogate models were developed with FEM model solutions, using different sampling schemes (regular grid, Monte Carlo sampling, Latin Hyper-cube sampling) and model approaches, N-dimensional cubic spline interpolation and Kriging. Repeated studies were used to quantify the well-posedness of the inversion problem, and the uncertainty was assessed in material property and crystallographic orientation estimates given typical geometric dimension variability in aerospace components. Surrogate model quality was found to be an important factor in inversion results when the model more closely represents the test data. One important discovery was when the model matches well with test data, a Kriging surrogate model using un-sorted Latin Hypercube sampled data performed as well as the best results from a N-dimensional interpolation model using sorted data. However, both surrogate model quality and mode sorting were found to be less critical when inverting properties from either experimental data or simulated test cases with uncontrolled geometric variation.

INTRODUCTION

Resonance Ultrasound Spectroscopy (RUS) is a method for non-destructive evaluation (NDE) and material characterization that uses the ultrasonic resonance frequencies of a component [1-2]. Vibrant Corporation combines RUS with advanced pattern recognition algorithms and statistical scoring to field Process Compensated Resonance Testing (PCRT) for commercial NDE applications [3]. Among the most critical of those applications are gas turbine engine blades made from nickel-based superalloys [4]. Previously for aerospace components, RUS-based inspections require a large quantity of empirical data in the form of resonance frequencies and part classifications to serve as a training set. Going forward, there is a critical need for quantitative models to more precisely relate changes in the material state with the resonance behavior of the material [5-6], reducing test specimen requirements.

Recent work has investigated enhancements of forward and inverse modeling capabilities for RUS. The application of the finite element method (FEM) to RUS forward and inverse modeling has addressed the representation of more complex shapes [7-9,6], certain damage conditions like creep [10-11] and varying crystal orientation with multiple grains [12]. While numerical models using FEM can successfully represent the resonance frequencies of complex parts, these models still have some error that will impact the inversion process and results. Sensitivity of RUS to small levels of geometric variation due to manufacturing tolerances is a concern. The use of a surrogate model (or meta-model) with FEM simulations has been investigated to increase RUS inversion solution time [6,13-14].

However, there is a need to better understand the impact of surrogate model quality on inversion error. Recent work has investigated quantifying the propagation of uncertainty in RUS frequency results for models and measurements [13-14]. Building on this prior work, a case study is presented on evaluating uncertainty in RUS inversion for a complex part, a single crystal (SX) Ni-based superalloy Mar-M247 cylindrical dog-bone specimen. In this paper, several surrogate models are developed with FEM model solutions using different sampling schemes. A process for evaluating the uncertainty propagation given variation in the geometry of a complex part is presented. Multiple metrics for inversion performance are studied, using both simulated and experimental data. Repeated studies were used to quantify the well-posedness of the inversion problem, and the uncertainty was assessed in material property and crystallographic orientation estimates given typical geometric dimension variability in aerospace components.

RUS MODEL-BASED INVERSION AND SOURCES OF UNCERTAINTY

A diagram of RUS model-based inversion is shown in Fig. 1(a), where RUS measured resonance frequencies are iteratively compared with a RUS model, to estimate the unknown material conditions and part states that are parameters of the model. For RUS inversion, two forms of uncertainty will be considered in this paper. Aleatory uncertainty characterizes the inherent randomness in the behavior of a system under study. For the RUS inverse model shown in Figure 1(a), aleatory uncertainty is associated with (1) material property, (2) part-to-part geometry, and (3) RUS test condition variation. In prior work [13], RUS measurement error was found to be well under control, while material property and geometry variation were found to drive uncertainty. Thus, the focus of this paper will focus on sensitivity to material and part geometry uncertainty. Epistemic uncertainty characterizes a lack of knowledge about the appropriate value to use for a quantity, assumed to have a fixed value. One example of epistemic uncertainty for RUS inversion is associated with (4) model uncertainty. Model error is frequently due to some un-modeled characteristic in the experiment, like the effect of the fixture at lower resonance frequencies. Lastly, the impact of inversion algorithm design will play a significant role in the resulting error / uncertainty of the inversion results. Such inversion parameters include (5) mode selection, potentially effecting uncertainty on mode matching, and (6) inversion (optimization) algorithm parameters. A focus of this work is to study the role of model error, mode selection / matching, and the inversion algorithm design on performance. Repeated studies, as shown in Figure 1(b), will be used to quantify the well-posedness of the inversion problem (loop 1), as well as the overall uncertainty in material property and crystallographic orientation estimates for uncertain material and part conditions (loop 2).

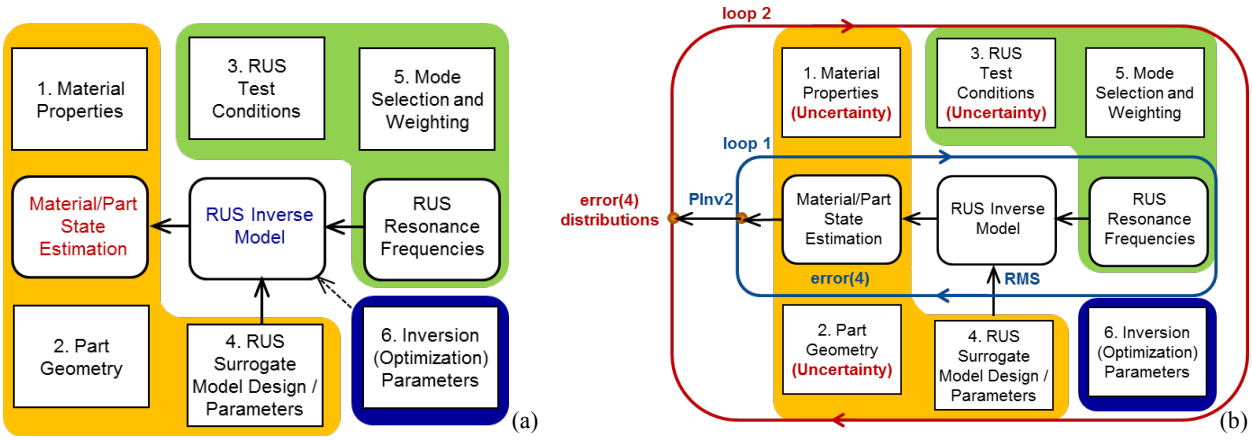

FIGURE 1. (a) Factors influencing RUS inverse model uncertainty. (b) Evaluation of inversion metrics through repeated studies: (loop 1) repeatability of convergence to a 'global' solution, and (loop 2) uncertainty distributions for parameter estimates.

SURROGATE MODELS AND DATA SAMPLING

Surrogate models can be generated using the results of numerical simulations to greatly improve the speed of inverse methods. Two approaches for surrogate modeling were considered in this paper: (1) N-dimensional interpolation, fitting cubic splines through a grid of simulated data, and (2) Kriging or Gaussian process regression models. Kriging is a method of interpolation for which the values are modeled by a Gaussian process governed by prior covariances, chosen to optimize the smoothness of the fit. The goal of considering Kriging as a surrogate model

was to address instances with more complexity of the parameter space, and handling irregular or randomly sampled parameter spaces. As well, kriging can generate surfaces that describe how well the model predicts between known points. The ooDACE Toolbox in Matlab was used to fit the forward modeling representation and was called by the inversion process [15]. The Matérn covariance function was used for the Kriging model, and pseudolikelihood option (as an alternative to Maximum Likelihood Estimation) was used to improve convergence of the Kriging regression fits. Note, to avoid some errors with Jacobian calculations using the Kriging model in Matlab, the default optimization algorithm properties were changed for 'FinDiffRelStep' to 10*eps^(1/3).

Three sampling approaches were also investigated: (1) regular spacing (grid), (2) random / Monte Carlo sampling (MC), and (3) Latin Hyper-Cube (LHC) sampling. Details on the sampling data sets are presented in Table 1. Five model parameters were varied throughout each study, three material properties representing the cubic single crystal (SX): E = Young's Modulus, nu (ν) = Poisson's Ratio, A = Anisotropy Ratio, and two representing the crystal orientation: beta (β) = angle rotated down from the z-axis, and gamma (γ) orientation about the z-axis [as shown in Figure 2(a)]. Baseline conditions for Mar-M247 used in the study are as follows: E = 127.42 GPa, nu = 0.385, A = 2.826, density = 8.55 g/cm^3, beta = 0°, and gamma = 0°. The upper and lower bounds for E', nu' and A' in Table 1 are essentially multipliers applied to this baseline properties. The range of variability in material properties for Mar-M247, ±5% for E and ±5% for A, follows prior work [16, 13], but wider bounds for nu, ±10% and beta were considered here. Note, for the variable, beta, additional factor levels (5) were necessary with regular grid spacing to address the complex simulated trends. Latin hypercube sampling is a statistical method for generating a near-random sampling of 'N' values from a multi-dimensional distribution [17]. A comparison of regular grid spacing (27×15 pts.) and LHC sampling (300 pts.) for the three material properties is shown in Figure 2(b) and 2(c) respectively. While this isn't a perfectly fair comparison since the true parameter space has 5 dimensions, but one can see how LHC can potentially address more subtle changes in the local parameter space. For all of the FEM RUS simulations in this study, COMSOL was used to generate numerical results for the first 100 resonance frequencies.

TABLE 1. Range of parameters for FEM simulations using three different sampling approaches.

	Sampling -> Parameters	Regular Spacing (grid)	Random / Monte Carlo (MC)	Latin Hypercube Sampling (LHC)
Parameters	N_runs	405	500	300
(1)	E' (multiplier)	[0.95 1.05] (3 levels)	[0.95 1.05]	[0.95 1.05]
(2)	nu' (multiplier)	[0.90 1.10] (3 levels)	[0.90 1.10]	[0.90 1.10]
(3)	A' (multiplier)	[0.95 1.05] (3 levels)	[0.95 1.05]	[0.95 1.05]
(4)	beta	[0 20] (5 levels)	[0 20]	[0 20]
(5)	gamma	[-45 45] (3 levels)	[-45 45]	[-45 45]

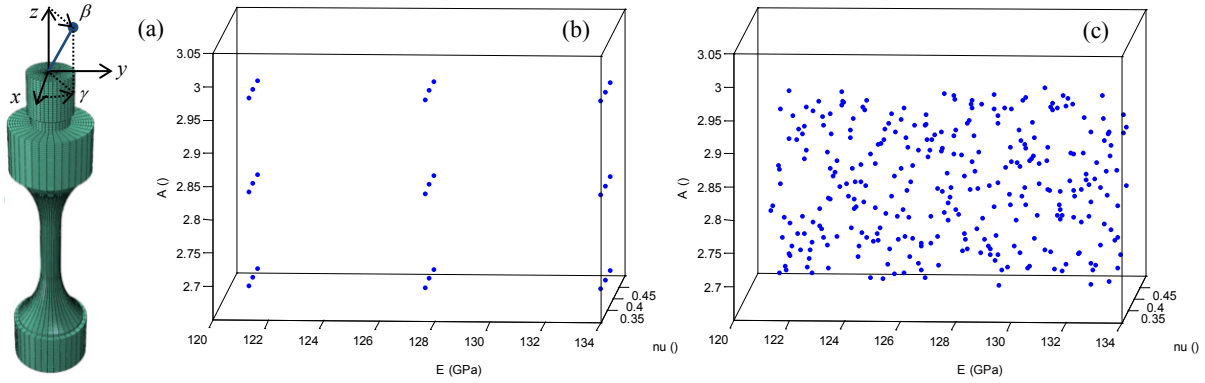

FIGURE 2. (a) Dog-bone coordinates. Distribution of (b) regular grid and (c) LHC sampling over cubic material parameters.

CHALLENGE CONCERNING MODE MATCHING

One challenge with building surrogate models for representing the resonance frequency response for a series of modes over varying material property and crystal orientation states is maintaining accuracy in the solution space at intermediate points. An example for one set of material properties (E' = 1.00, nu' = 1.00, A' = 1.05, gamma = 0°) with

varying crystal orientation angle, beta, is presented in Figure 3(a). For modes 11 to 14, they are close in frequency, and found to switch order with varying angle beta. Ideally, the goal in developing surrogate models is to sample the FEM model using a limited number of calls, for example using a regular grid from 0° to 20° in 5° steps. Finer studies with varying beta were also run and are superimposed over these regular step points, showing the actual underlying trend between these intermediate points. Prior work has investigated the use of mode shape information on RUS inversion [18] using laser vibrometry measurements, but this issue with swapping modes in surrogate models [13] has frequently been addressed manually to date. One approach that has been proposed is to use mode matching metrics based on the mode shapes, which would then enable proper model interpolation between intermediate solutions points. One good example of how mode matching can be successful is shown for the modes in Figure 3(d), 3(e), 3(h) and 3(i). Here, mode matching can be used to track the switch in modes 13 and 14 at beta = 6°. However, only relying on mode shape matching has been found to be quite problematic when varying crystal orientation is present. One example where mode matching breaks down is shown for the mode shapes in Figure 3(g), 3(h), 3(j) and 3(l) (see arrows in plot). Between 10° and 15°, the 'mode shapes' actually switch between mode 12 and mode 14 curves. Thus, if an attempt was made to interpolate between these FEM solution points, the intermediate solutions would be in error. This matching problem is also complicated in this range because of a switch also occurring between modes 11 and 12 between 10° and 15°. One switch requires reliance on matching mode shapes, while the other does not. While finer steps in the simulations relative to the changing parameter could improve the tracking of modes, the downside is more FEM simulation points would be required. Thus, one objective of this study is to evaluate the necessity of mode matching in the surrogate model build.

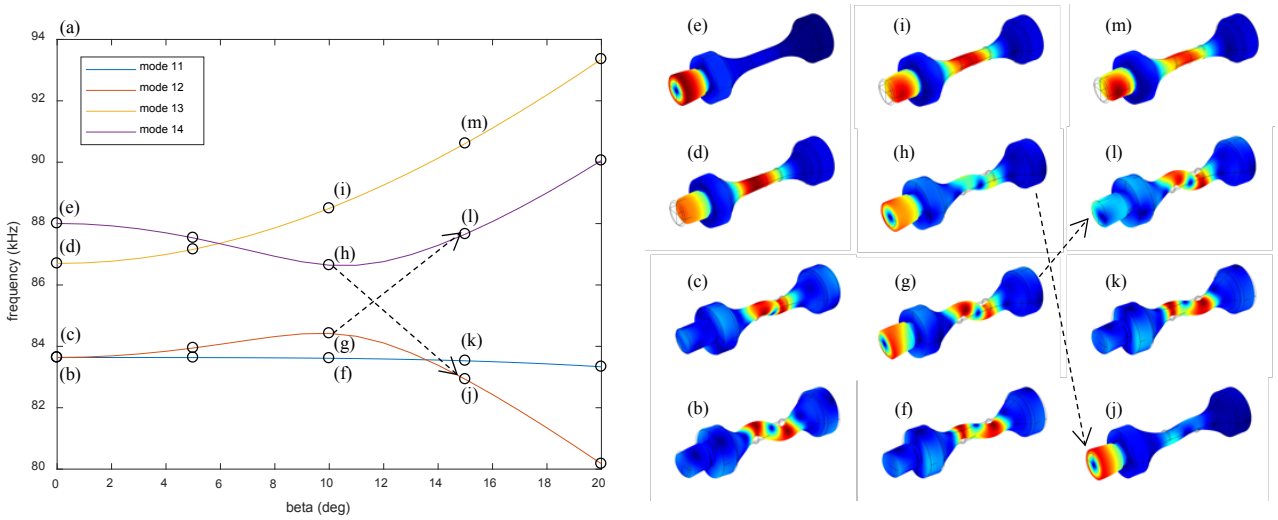

FIGURE 3. (a) Plot of simulated frequencies for modes 11 – 14 for the SX dog-bone specimen with varying angle beta. (b)-(e) Mode shapes 11-14 for beta = 0°, (f)-(i) mode shapes 11-14 for beta = 10° and (j)-(m) mode shapes 11-14 for beta = 15°.

STUDY METRICS

Prior work has investigated a variety of metrics to evaluate the performance of inverse methods [19-21]. A diagram of the evaluation of key metrics with respect to the RUS inverse problem is presented in Fig. 1(b). First, error metrics on the residual between the model fit and experimental data are useful as a relative measure of the model fit quality. Root mean squared (RMS) error of the measured data to the best-fit forward model is given as follows:

$$RMS = \sqrt{\frac{1}{n}\sum_{i=1}^{n}(f_i^e - f_i^m)^2}, \quad (1)$$

where n is the total number of samples, and f_i^e and f_i^m are the experimental and modeled frequencies respectively. A second metric used throughout this paper is simply a 'composite' error metric on the four key parameters being estimated through the inverse problem:

$$\text{error4} = \frac{1}{4}(dE + dnu + dA + dbeta), \quad (2)$$

where *dE, dnu, dA* are in 'percent error' for Young's Modulus, Poisson's Ratio, and Anisotropy Ratio respectively, while *dbeta* is normalized (error in angle / 1°). (The issue is that one cannot normalize errors in angle on a percentage basis, so a normalizing factor is needed.) Note, uncertainty on the parameter estimates is also considered in this study. Using repeated studies, as shown in Figure 1(b), the overall uncertainty in material property and crystallographic orientation can be evaluated (see loop 2) through considering uncertainty in the material properties and part conditions.

Lastly, the third metric of interest is defined as PInvC2, the Probability of Inversion Convergence. Ideally, one would like to report the likelihood of convergence to the 'global' solution. However, it is of course difficult to make this strong statement, and at best one can only evaluate the frequency of converging to the best solution given some 'bounds' on accuracy. Note, this metric was studied in [20] for an eddy current inverse problem. Unfortunately, the estimation of confidence bounds on inversion results (based on regression error and model sensitivity relative to the parameter space) was found to be non-conservative because the underlying assumptions were frequently invalid. A proposed new metric, PInvC2 simply evaluates the percentage of instances of achieving the best solution using Monte Carlo simulations with 50 random initial guesses (as shown in loop 1). However, an alternative fixed bound criterion was set here, based on a percent basis, relative to the range (max. and min.) of possible parameter values, of ± 0.01%.

RESULTS

Study 1 - Effect of Surrogate Model Design and Simulated Data Sampling

Results investigating the effect of surrogate model design and data sample number are presented in Table 2. The table error results represent the average of inversion error over 20 new simulated data samples, independent of the grid, MC and LHC simulated studies. First, several initial statements can be made about the importance of mode sorting (columns 1-3) for regular grid data. Perfectly sorted data does improve inversion performance with N-dimensional interpolation, relative to unsorted data. Interestingly, partially sorted data, using an automated mode matching algorithm but including some errors as shown in Figure 3, were found to cause more harm than good.

Concerning results for Kriging models, they were found to perform best at inverting intermediate data points in the solution space when trained using MC or LHC sample data sets. Increased sampling was found to generally improve Kriging results. LHC Sampling appears to be most efficient, with low error4, while using only 300 samples. Note, the Kriging fit was especially poor for the regular grid data, primarily due to the sparse spacing (see Figure 2).

Several interesting observations can be made about the use of Kriging for surrogate models versus N-dimensional interpolation. A Kriging model fit using un-sorted data (column 7) perform as well as the best results from N-dimensional interpolation models using mode-matched (sorted) data (column 3). The rate of convergence to the global solution, PInvC2, was good (~90%) and generally similar for models built with un-sorted and sorted data. These results are especially important due to the burden of achieving quality sorted RUS mode data over a wide range of parametric (material property and crystal orientation) conditions. Clearly, there are advantages with using Kriging with randomly sampled spaces, able to represent the complex mode trends with limited error, as shown in Figure 3(a).

TABLE 2. Inversion results for varying surrogate model and sample number, averaged over 20 known simulated test cases.

surrogate model design	1. grid, no sort, Ninterp	2. grid, part/sort, Ninterp	3. grid, sorted, Ninterp	4. grid, no sort, Kriging	5. grid, part/sort, Kriging	6. grid, sorted, Kriging	7. LHC, no sort, Kriging	8. MC, no sort, Kriging	9. MC2 no sort, Kriging	10. MC3 no sort, Kriging	11. MC5 no sort, Kriging
sample#	405	405	405	405	405	405	300	500	300	405	905
dE	0.106	0.177	0.036	0.717	0.814	0.852	0.040	0.036	0.105	0.046	0.037
dnu	0.255	0.501	0.112	0.845	1.136	0.927	0.091	0.593	0.042	0.120	0.060
dA	0.287	0.596	0.101	1.741	1.994	2.006	0.124	0.498	0.517	0.386	0.098
dbeta	0.313	0.371	0.137	0.977	0.997	1.034	0.087	0.060	0.060	0.056	0.070
dgamma	22.0	18.5	21.9	24.0	23.2	23.3	29.7	9.2	6.4	9.1	10.8
%error4	0.240	0.411	0.097	1.070	1.235	1.205	0.086	0.297	0.181	0.152	0.066
PInvC2	0.940	0.800	0.878	0.834	0.662	0.738	0.879	0.896	0.872	0.947	0.862
RMS	0.052	0.073	0.020	0.198	0.223	0.198	0.020	0.011	0.012	0.011	0.010

Inversion results are presented in Table 3, averaged over a set of experimental results from 7 RUS data sets, acquired using repeated measurements of 4 SX dog-bone specimens (A,E,I,K). More details on these specimens can be found in [6]. First, there is very little difference in the RMS fit for all of the surrogate models. For this study, the surrogate model-to-model differences are very small compared to the systematic differences between FEM models and the experimental fit modes. Note, RMS values are essentially an order of magnitude larger than the inversion results for the known 'simulated' test data. Thus, when more error exists between the model and experimental modes, high model quality becomes less important. Results are presented in Table 4 using the two 'better' surrogate model designs (case 3 and 11), for 7 unknown experimental test cases. Note, near agreement was observed between the two best surrogate models: (3) Ninterp, sorted data, and (11) Kriging w/905 random samples. Future work is planned to verify the observed crystal orientation differences between specimen 'E' and the other three specimens sets.

TABLE 3. Inversion results for varying surrogate model and sample number, averaged over 7 unknown experimental test cases.

surrogate model design	1. grid, no sort, Ninterp	2. grid, part/sort, Ninterp	3. grid, sorted, Ninterp	4. grid, no sort, Kriging	5. grid, part/sort, Kriging	6. grid, sorted, Kriging	7. LHC, no sort, Kriging	8. MC, no sort, Kriging	9. MC2 no sort, Kriging	10. MC3 no sort, Kriging	11. MC5 no sort, Kriging
sample#	405	405	405	405	405	405	300	500	300	405	905
dE'	0.84	0.70	0.82	0.66	0.51	0.92	0.83	0.72	0.82	0.77	0.81
dnu'	1.75	1.00	1.66	1.36	5.17	3.83	1.91	2.42	1.66	1.86	1.73
dA'	4.87	4.90	4.87	5.00	5.00	4.68	4.90	4.80	4.79	4.81	4.85
beta'	7.17	6.87	7.09	6.89	6.40	7.13	7.06	6.96	6.88	6.92	7.08
PInvC2	1.000	0.996	0.997	1.000	0.958	0.994	1.000	1.000	1.000	1.000	1.000
RMS	0.541	0.541	0.548	0.596	0.525	0.522	0.548	0.546	0.540	0.546	0.551

TABLE 4. Inversion results using two 'better' surrogate model designs, for 7 unknown experimental test cases.

surrogate model design	specimen	A1	E1	E2	I_mean	K_mean	A_mean	E_mean
3. grid, sorted, Ninterp	E (GPa)	126.35	126.47	126.62	126.05	126.27	126.35	126.56
3. grid, sorted, Ninterp	nu ()	0.375	0.382	0.384	0.378	0.374	0.375	0.382
3. grid, sorted, Ninterp	A ()	2.685	2.685	2.685	2.711	2.685	2.685	2.685
3. grid, sorted, Ninterp	beta (deg.)	6.66	8.01	7.39	6.68	6.45	6.74	7.68
11. MC5 no sort, Kriging	E (GPa)	126.37	126.48	126.63	126.04	126.27	126.37	126.57
11. MC5 no sort, Kriging	nu ()	0.374	0.382	0.384	0.377	0.374	0.375	0.382
11. MC5 no sort, Kriging	A ()	2.685	2.685	2.685	2.714	2.685	2.685	2.685
11. MC5 no sort, Kriging	beta (deg.)	6.63	8.01	7.40	6.64	6.44	6.72	7.68

Study 2 - Effect of Uncontrolled Geometric Variation

The goal of the second study was to evaluate the effect of uncontrolled geometric variation for the RUS test specimen and inversion algorithm design on the material property and crystal orientation (E, nu, A, beta) inversion results. For aerospace propulsion components, typical manufacturing tolerances of ±0.05 mm (~ ± 2 mils) were considered for this study. Three simulated data sets were constructed exploring both material and geometric variation:

1. One-factor-at-a-time (OFAT) studies: 20 sets of material properties configurations were first randomly sampled from the material property / crystal orientation space. For each of these 20 property sets, one baseline simulation and 8 OFAT dimensional parameter changes were run. (20 * 9 = 180 simulations).
2. Monte Carlo (MC) sampling using uniform distributions (between ±0.05 mm) of the part dimensions: 20 sets of material properties configurations were sampled from the property space. For each of these 20 property sets, 20 random dimensions samples were made over the eight parameters. (20 * 20 = 400 simulations).
3. Monte Carlo (MC) sampling using Gaussian distributions of the part dimensions (where ±0.05 mm = ±2σ): 20 sets of material properties configurations were sampled from the property space. For each of these 20 property sets, 40 random dimensions samples were made over the eight parameters. (20 * 40 = 800 simulations).

Figure 4 presents the 8 parameters that were varied in the studies, with the corresponding 'percent change' based on +0.05 mm tolerance. Note, fixed dimension accuracy has the greatest impact, in terms of a percentage change, on

thinnest section of cylindrical dog-bone, with a change of 2.5%. This large percentage change will be reflected in the effect on certain modes, more than others, and subsequently the accuracy of the inversion results. Inversion results are presented in Table 5 for varying select geometric properties OFAT (averaged over 20 simulated test cases) using both good (col. 3 and 11) and poorer (col. 1 and 9) surrogate models. Diameter changes in the thinnest section of the dog-bone clearly produced the largest error in property estimates. On a percent basis, such small length changes of 0.05 mm can thus have a sizable effect on material property estimates, when they occur in the most sensitive portion of the specimen. In general, changes in nu and A were shown to be greater than E with uncontrolled part variation. Surrogate model selection was found to have very little effect on the results when 'uncontrolled' dimension variation of the part is also present, similar to working with experimental test specimens. Only when the model is an excellent fit to the 'test' data, does surrogate model quality appear to make a difference.

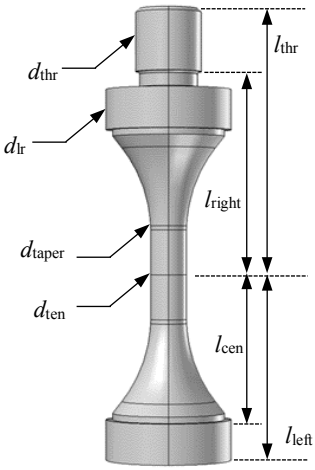

#	Dog-bone Parameters	Name	Orig Dim (mm)	Add 0.05 (mm)	% Change
1	center length	l_cen	16.18	16.23	0.31%
2	left section length	l_left	20.68	20.73	0.24%
3	right section length	l_right	22.68	22.73	0.22%
4	thread length	l_thr	29.72	29.77	0.17%
5	center radius	d_cen	2.000	2.050	2.50%
6	left/right radius	d_lr	7.000	7.050	0.71%
7	thread radius	d_thr	3.680	3.730	1.36%
8	taper radius	d_taper	2.207	2.257	2.27%

FIGURE 4. Dog-bone geometry model in COMSOL considering geometric variation of eight parameters.

TABLE 5. Inversion results for varying select geometric properties (over 20 simulated test cases) using good and poorer models.

	baseline	**l_cen**	**l_left**	**l_right**	**l_thr**	**d_cen**	**d_taper**	**d_lr**	**d_thr**
surrogate	**good (3, 11)**	**good (3, 11)**	**good (3, 11)**	**good (3, 11)**	**good (3, 11)**	**good (3, 11)**	**good (3, 11)**	**good (3, 11)**	**good (3, 11)**
E_err	0.037	0.152	0.201	0.037	0.106	0.584	0.765	0.815	0.084
nu_err	0.111	1.267	0.814	0.310	0.904	1.821	4.389	2.066	0.555
A_err	0.100	0.630	1.205	0.401	0.860	2.489	0.889	1.777	0.192
beta_err	0.094	0.219	0.180	0.118	0.157	2.034	0.812	0.305	0.102
error4	0.085	0.567	0.600	0.217	0.507	1.732	1.714	1.241	0.233
PInvC2	0.861	0.972	0.948	0.937	0.946	1.000	0.999	0.985	0.875
RMS	0.020	0.102	0.100	0.037	0.087	0.427	0.373	0.201	0.028
surrogate	**poor (1, 9)**	**poor (1, 9)**	**poor (1, 9)**	**poor (1, 9)**	**poor (1, 9)**	**poor (1, 9)**	**poor (1, 9)**	**poor (1, 9)**	**poor (1, 9)**
error4	0.184	0.524	0.646	0.222	0.513	1.598	1.771	1.275	0.281
PInvC2	0.948	0.979	0.988	0.985	0.985	0.983	0.997	0.996	0.941
RMS	0.043	0.109	0.104	0.053	0.093	0.419	0.369	0.203	0.046

Table 6 presents the average inversion results varying the eight geometric properties using a Monte Carlo study (1) with a uniform distribution of ±0.05 mm. Again, surrogate model quality was found to have very little effect on the results when 'uncontrolled' dimension variation is also present. Following the approach presented in Figure 1(b) (loop 2), error distributions were evaluated for Young's Modulus, Poisson's Ratio, Anisotropy Ratio, and beta, over 1600 inversions, in Figure 5 and 6, assuming uniform and Gaussian input distributions for the geometric parameters respectively. As expected, error distributions appeared more 'normal' for Gaussian sampling versus uniform sampling. One concern is the large level of error, especially in nu and A. Clearly, if more accurate inversions are desired for aerospace components, reducing uncertainty in the geometric properties of the specimens is critical.

Lastly, Fig. 7 presents the relationship between the RMS error and the inversion error (error4) for the 1600 inversion solutions from Monte Carlo study (2) with Gaussian sampling for geometric uncertainty, using results from

2 surrogate models (col. 3 and 11). For this study, RMS error does not predict well the accuracy of estimated material properties (error4). The R^2 metric of how close the data are to the fitted regression line was found to be poor, 0.1995.

TABLE 6. Inversion results varying surrogate model for a Monte Carlo study (uniform distributions) of geometric properties

surrogate model design	1. grid, no sort, Ninterp	3. grid, sorted, Ninterp	10. MC3 no sort, Kriging	11. MC5 no sort, Kriging
sample#	405	405	405	905
dE	0.668	0.598	0.615	0.616
dnu	3.078	3.030	3.035	3.037
dA	1.686	1.521	1.563	1.517
dbeta	1.296	1.330	1.288	1.343
%error4	1.682	1.620	1.625	1.628
PInvC2	0.993	0.985	0.987	0.997
RMS	0.346	0.344	0.339	0.342

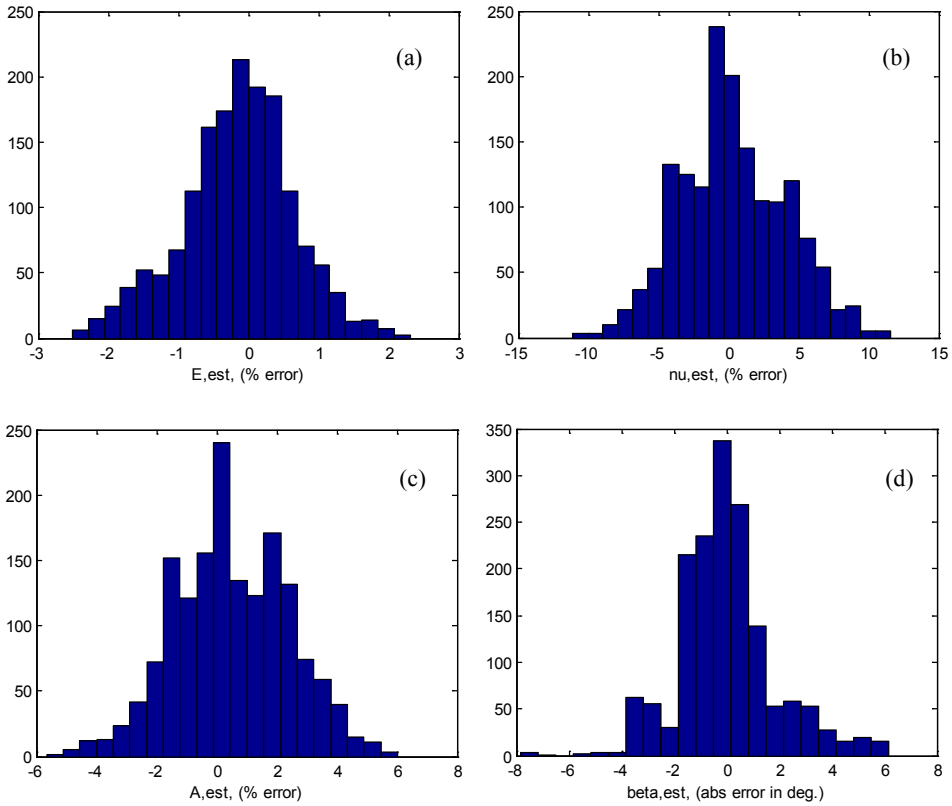

FIGURE 5. Error distributions of estimated parameter results: (a) E = Young's Modulus, (b) nu = Poisson's Ratio, (c) A = Anisotropy Ratio, (d) beta = single crystal orientation, over 1600 inversions with uniform input distributions.

CONCLUSIONS AND FUTURE WORK

In this paper, a case study is presented evaluating error in RUS inversion for a single crystal (SX) Ni-based superalloy Mar-M247 cylindrical dog-bone specimens. A number of surrogate models were developed with FEM model solutions, using different surrogate modeling approaches and sampling schemes. Surrogate model quality was found to be an important factor in inversion results when the model more closely represents the 'test' data. One

important discovery was when model quality is critical, a Kriging model fit using un-sorted Latin Hypercube sampled data performed as well as the best results from a N-dimensional interpolation model using sorted data. However, both the surrogate model and mode sorting were found to be less critical when inverting properties of either experimental data or simulated test cases with uncontrolled geometric variation. To improve inversion accuracy when model quality does not represent the test parts well, future work is planned to build on recent progress on Part-to-Itself (PTI) model inversion [22], fitting to differences from a designated reference sample rather than absolute property values, yielding a reduction in fit error and improved parameter estimation.

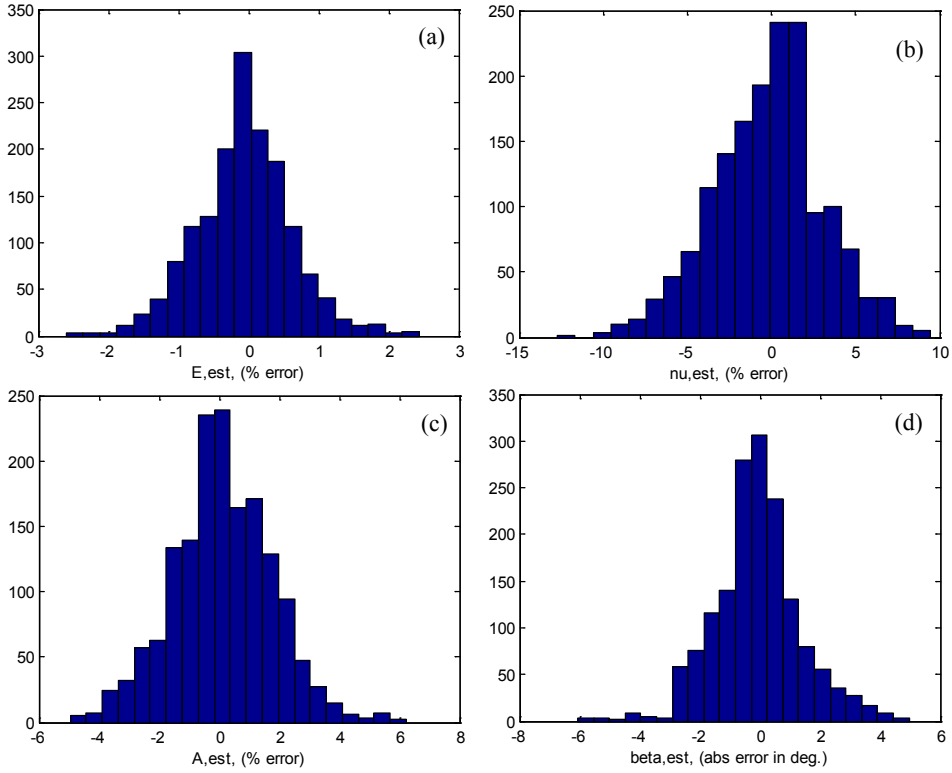

FIGURE 6. Error distributions of estimated parameter results: (a) E = Young's Modulus, (b) nu = Poisson's Ratio, (c) A = Anisotropy Ratio, (d) beta = single crystal orientation, over 1600 inversions with Gaussian input distributions.

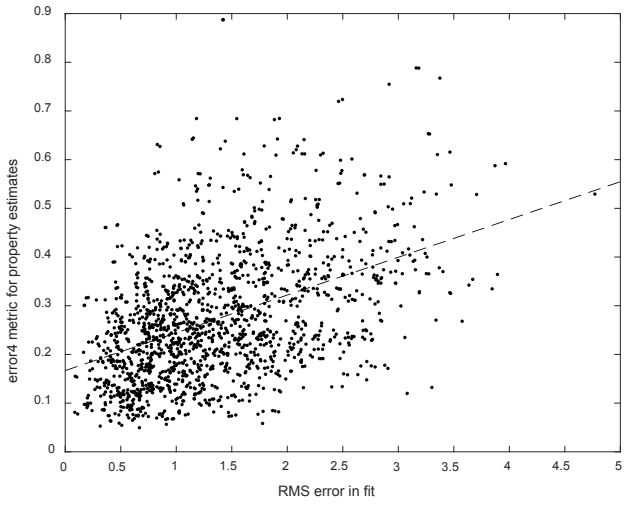

FIGURE 7. Relationship between error in material property estimation (error4) and RMS error in mode fit.

ACKNOWLEDGMENTS

This research was supported by the U.S. Air Force Research Laboratory (AFRL) through a Materials and Manufacturing Director (AFRL/RX) Structural Materials Broad Agency Announcement (BAA) Contract FA8650-15-M-5208 and an AFRL Small Business Innovation Research (SBIR) Phase II Contract, FA8650-15-M-5074.

REFERENCES

1. A. Migliori, J. Sarrao, M. W. Visscher, T. Bell, M. Lei, Z. Fisk, and R. Leisure, ‘‘Resonant ultrasound spectroscopy techniques for measurement of the elastic moduli of solids,’’ *Physica B*, **183**, 1–24 (1993).
2. A. Migliori, and J. L. Sarrao, *Resonant Ultrasound Spectroscopy*, New York, Wiley, (1997).
3. J. Schwarz, J. Saxton, and L. Jauriqui, “Process compensated resonant testing in manufacturing process control,” *Material Evaluation*, **63,** pp. 736-739, (July 2005).
4. D. Piotrowski, L. Hunter, and T. Sloan, “Process compensated resonance testing JT8D-219 1st stage blades,” ATA NDT Forum 2008, (September 24, 2008).
5. J. C. Aldrin, L. Jauriqui, and L. Hunter, “Models for process compensated resonant testing (PCRT) of silicon nitride balls,” *Review of Progress in QNDE*, Vol. 32, AIP Conf. Proc, **1511**, pp.1393-1400, (2013).
6. E. Biedermann, et al., “Resonance ultrasound spectroscopy forward modeling and inverse characterization of nickel-based superalloys,” *41st Annual Review of Progress in QNDE*, AIP Conf. Proc, **1650**, pp. 835-844, (2015).
7. J. Plesek, R. Kolman, and M. Landa, “Using finite element method for the determination of elastic moduli by resonant ultrasound spectroscopy,” *Journal of the Acoustical Society of America*, **116**, No. 1, pp. 282-287, (2004).
8. G. Liu, and J. D. Maynard, “Measuring elastic constants of arbitrarily shaped samples using resonant ultrasound spectroscopy,” *Journal of the Acoustical Society of America*, **131**, No. 3, pp. 2068-2078, (2012).
9. M. C. Remmillieux, T. J. Ulrich, C. Payan, J. Riviere, C. R. Lake, and P.-Y. Le Bas, “Resonant ultrasound spectroscopy for materials with high damping and samples with arbitrary geometry,” *Journal of Geophysical Research: Solid Earth*, **120**, pp. 4898-4916, (2015).
10. B. R. Goodlet, C. J. Torbet, E. Biedermann, L. Jauriqui, J. C. Aldrin, T. M. Pollock, “Forward models for extending the mechanical damage evaluation capability of resonant ultrasound spectroscopy,” *Ultrasonics*, **77**, 183-196, (2017).
11. J. Heffernan, L. Jauriqui, E. Biedermann, A. Mayes, R. Livings, B. Goodlet, and S. Mazdiyasni, “Process compensated resonance testing models for quantification of creep damage in single crystal nickel-based superalloys” *Materials Evaluation*, **75**, n 7, pp. 941-952, (2017).
12. T. J. Lesthaeghe, R. A. Adebisi, S. Sathish, M. R. Cherry, and P. A. Shade, “Toward characterization of single crystal elastic properties in polycrystalline materials using resonant ultrasound spectroscopy,” *Materials Evaluation*, **75**, n 7, pp. 930-940, (2017).
13. E. Biedermann, L. Jauriqui, J. C. Aldrin, A. Mayes, T. Williams, and S. Mazdiyasni, “Uncertainty quantification in modeling and measuring components with resonant ultrasound spectroscopy,” *42nd Annual Review of Progress in QNDE,* AIP Conf. Proc, **1706**, p. 070008, AIP Publishing, (2016).
14. E. Biedermann, J. Heffernan, A. Mayes, G. Gatewood, L. Jauriqui, B. Goodlet, S. Mazdiyasni, “Process compensated resonance testing modeling for damage evolution and uncertainty quantification,” *43rd Annual Review of Progress in QNDE,* AIP Conf. Proc, **1806**, p. 090005 (2017).
15. I. Couckuyt, T. Dhaene, and P. Demeester. "ooDACE toolbox: a flexible object-oriented Kriging implementation." *Journal of Machine Learning Research*, **15**, pp. 3183-3186 (2014).
16. H-A. Kuhn, and H-G Sockel, “Elastic properties of textured and directionally solidified nickel-based superalloys between 25 and 1200° C,” *Materials Science and Engineering, A112,* 177-126, (1989).
17. M. D. McKay, R. J. Beckman, and W. J. Conover. "Comparison of three methods for selecting values of input variables in the analysis of output from a computer code." *Technometrics*, **21**, n 2, pp. 239-245, (1979).
18. H. Ogi, P. Heyliger, H. Ledbetter, and S. Kim, “Mode-selective resonance ultrasound spectroscopy of a layered parallelepiped,” *Journal of the Acoustical Society of America*, **108** (6), pp. 2829-2834, (2000).
19. J. C. Aldrin, J. S. Knopp, M. P. Blodgett, and H. A. Sabbagh, “Uncertainty propagation in eddy current inverse problems”, *Review of Progress in QNDE,* Vol. 30, AIP Conf. Proc., **1335**, pp. 631-638, (2011).
20. J. C. Aldrin, H. A. Sabbagh, C. Annis, E. B. Shell, J. Knopp, and E. A. Lindgren, “Assessing inversion performance and uncertainty in eddy current crack characterization applications,” *Review of Progress in QNDE*, Vol. 34, AIP Conf. Proc., **1650**, pp. 1873-1883, (2015).
21. H. T. Banks, S. Hu, W. C. Thompson, *Modeling and Inverse Problems in the Presence of Uncertainty*, CRC Press, (2014).
22. A. Mayes, L. Jauriqui, E. Biedermann, J. Heffernan, R. Livings, J. C. Aldrin, B. Goodlet, S. Mazdiyasni, “Part-to-itself (PTI) model inversion in process compensated resonance testing (PCRT),” *44th Annual Review of Progress in QNDE*, AIP Conf. Proc., (expected, 2018).